Making Convolutional Networks Shift-Invariant Again

Richard Zhang [1]

Abstract

Modern convolutional networks are not shift-invariant, as small input shifts or translations can cause drastic changes in the output. Commonly used downsampling methods, such as max-pooling, strided-convolution, and average-pooling, ignore the sampling theorem. The well-known signal processing fix is anti-aliasing by low-pass filtering before downsampling. However, simply inserting this module into deep networks leads to performance degradation; as a result, it is seldomly used today. We show that when integrated correctly, it is compatible with existing architectural components, such as max-pooling. The technique is general and can be incorporated across layer types and applications, such as image classification and conditional image generation. In addition to increased shift-invariance, we also observe, surprisingly, that anti-aliasing boosts accuracy in ImageNet classification, across several commonly-used architectures. This indicates that anti-aliasing serves as effective regularization. Our results demonstrate that this classical signal processing technique has been undeservingly overlooked in modern deep networks. Code and anti-aliased versions of popular networks will be made available at https://richzhang.github.io/antialiased-cnns/.

1. Introduction

When downsampling a signal, such an image, the textbook solution is to anti-alias by low-pass filtering the signal (Oppenheim et al., 1999; Gonzalez & Woods, 1992). Without it, high-frequency components of the signal alias into lower-frequencies. This phenomenon is commonly illustrated in movies, where wheels appear to spin backwards, known as the Stroboscopic effect, due to the frame rate not meeting the classical sampling criterion (Nyquist, 1928). Interestingly, most modern convolutional networks do not worry about anti-aliasing.

---
[1]Adobe Research, San Francisco. <rizhang@adobe.com>.

Early networks did employ a form of blurred-downsampling – average pooling (LeCun et al., 1990). However, ample empirical evidence suggests max-pooling provides stronger task performance (Scherer et al., 2010), leading to its widespread adoption. However, max-pooling does not provide the same anti-aliasing capability, and a curious, recently uncovered phenomenon emerges – small shifts in the input can drastically change the output (Engstrom et al., 2017; Azulay & Weiss, 2019). As illustrated in Fig. 1, network outputs can oscillate depending on the input position.

Blurred-downsampling and max-pooling are commonly viewed as competing downsampling strategies (Scherer et al., 2010). However, we show that the techniques are compatible. Our simple observation is that max-pooling is inherently composed of two operations: (1) evaluating the max operator densely and (2) naive subsampling. We propose to add a low-pass filter between the two. This viewpoint enables low-pass filtering to augment, rather than replace max-pooling. As a result, shifts in the input leave the output relatively unaffected (shift-invariance) and more closely shift the internal feature maps (shift-equivariance).

Furthermore, this enables proper placement of the low-pass filter, directly before subsampling. With this methodology, practical anti-aliasing can be achieved with any existing strided layer, such as strided-convolution.

A potential concern is that overaggressive filtering can result in heavy loss of information, causing performance degradation. However, with a reasonable selection of low-pass filter weights, we actually observe an *increase* in absolute performance in ImageNet classification (Russakovsky et al., 2015), across architectures. We additionally test on an image-to-image translation task, where generating high-frequency content is critical for high-quality results. In summary, our contributions are as follows:

- We integrate classic anti-aliasing filtering to improve shift-equivariance/invariance of deep networks. Critically, the method does not necessitate replacement of any existing downsampling strategy, such as max-pooling.
- We validate on common downsampling strategies – max-pooling, average-pooling, strided-convolution – in different architectures. We test across multiple tasks – image classification and image-to-image translation.
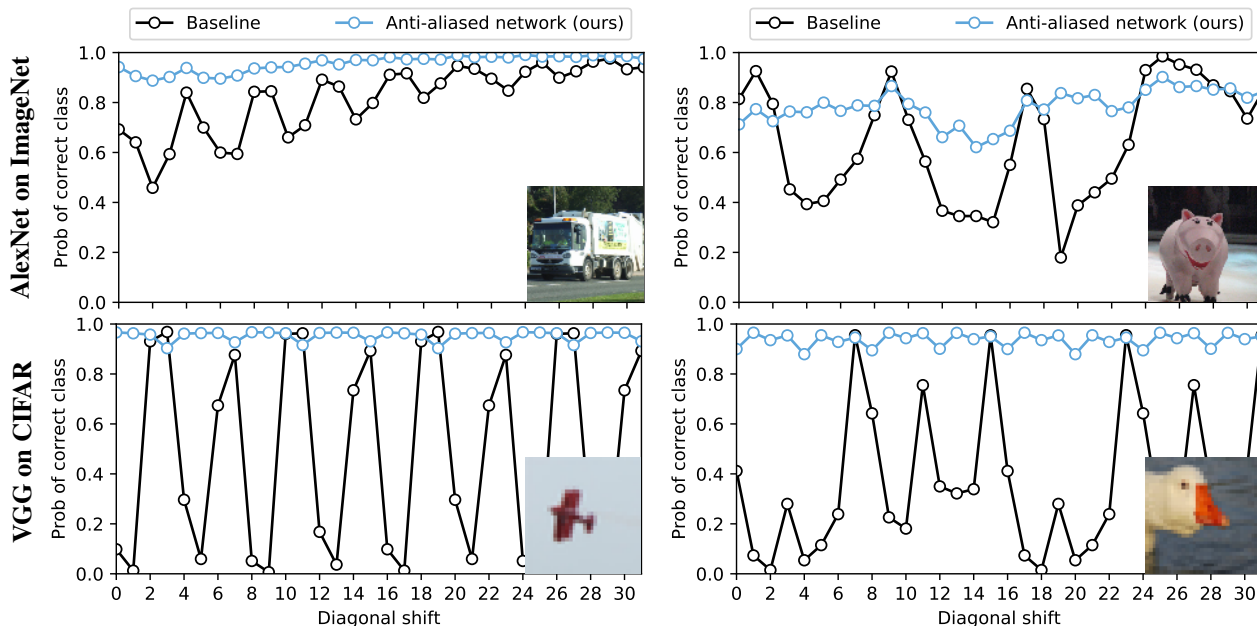- For ImageNet classification, we find, surprisingly, that

Figure 1. **Classification stability for selected images.** Predicted probability of the correct class changes when shifting the image. The baseline (black) exhibits chaotic behavior, which is stabilized by our method (blue). We find this behavior across networks and datasets. Here, we show selected examples using an AlexNet architecture on ImageNet **(top)** and a VGG architecture on CIFAR10 **(bottom)**.

classification accuracy actually increases, indicating that low-pass filtering serves as an effective regularizer.

2. Related Work

Local connectivity and weight sharing have been a central tenet of neural networks, including the Neocognitron (Fukushima & Miyake, 1982), LeNet (LeCun et al., 1998) and modern networks such as Alexnet (Krizhevsky et al., 2012), VGG (Simonyan & Zisserman, 2015), ResNet (He et al., 2016), and DenseNet (Huang et al., 2017). In biological systems, local connectivity was famously discovered in a cat's visual system (Hubel & Wiesel, 1962). Recent work has strived to build in additional types of invariances, such as rotation, reflection, and scaling (Sifre & Mallat, 2013; Bruna & Mallat, 2013; Esteves et al., 2018; Kanazawa et al., 2014; Worrall et al., 2017; Cohen & Welling, 2016). Our focus is on shift-invariance, a property often taken for granted.

Though different properties and invariances have been engineered into networks, what factors and invariances does an emergent representation actually learn? Analysis of deep networks have included qualitative approaches, such as showing patches which activate hidden units (Girshick et al., 2014; Zhou et al., 2015), actively maximizing hidden units (Mordvintsev et al., 2015), and mapping features back into pixel space (Zeiler & Fergus, 2014; Hénaff & Simoncelli, 2016; Mahendran & Vedaldi, 2015; Dosovitskiy & Brox, 2016a;b; Nguyen et al., 2017). Our analysis is focused on a specific, low-level property and is complementary to these qualitative approaches.

A more quantitative approach for analyzing networks is measuring representation or output changes (or robustness to changes) in response to manually generated perturbations to the input, such as image transformations (Goodfellow et al., 2009; Lenc & Vedaldi, 2015; Azulay & Weiss, 2019), geometric transforms (Fawzi & Frossard, 2015; Ruderman et al., 2018), and CG renderings with various shape, poses, and colors (Aubry & Russell, 2015). A related line of work is adversarial examples, where input perturbations are purposely directed to produce large changes in the output. These perturbations can be on pixels (Goodfellow et al., 2014a;b), a single pixel (Su et al., 2019), small deformations (Xiao et al., 2018), or even affine transformations (Engstrom et al., 2017). We aim to make the network robust to the simplest of these types of attacks and perturbations: shifts.

Classic hand-engineered computer vision and image processing representations, such as SIFT (Lowe, 1999), wavelets, and image pyramids (Adelson et al., 1984; Burt & Adelson, 1987) also extract features in a sliding window manner, often with some subsampling factor. As discussed in Simoncelli et al. (1992), literal shift-equivariance cannot hold when subsampling. Shift-equivariance can be recovered if features are extracted densely, for example textons (Leung & Malik, 2001), the Stationary Wavelet Transform (Fowler, 2005), and DenseSIFT (Vedaldi & Fulkerson, 2008). Deep networks can also be evaluated densely, by removing striding and making appropriate changes to subsequent layers by using *á trous*/dilated convolutions (Chen
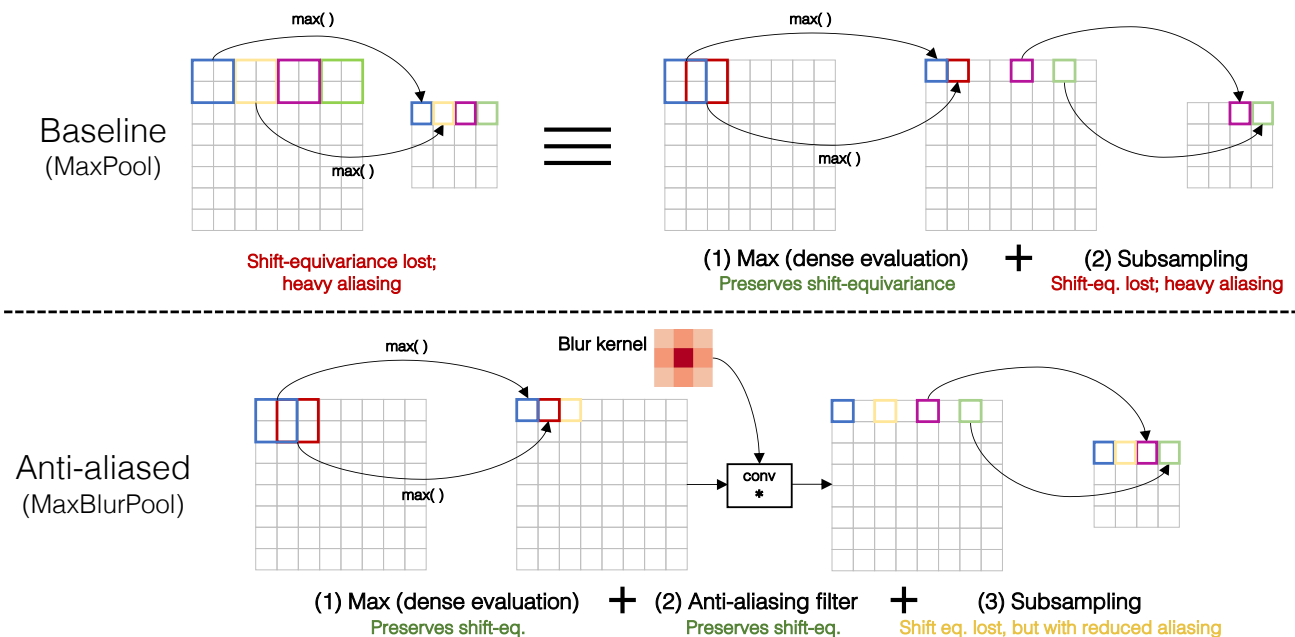
Figure 2. **Anti-aliasing convolutional networks. (Top)** Pooling does not preserve shift-equivariance. It is functionally equivalent to densely evaluated pooling followed by subsampling. The latter operation ignores the Nyquist sampling theorem and loses shift-equivariance. **(Bottom)** We low-pass filter between the operations. This keeps the original pooling operation, while anti-aliasing the appropriate signal. This equivalent analysis and modification can be applied to any strided layer – we experiment with **MaxPool→MaxBlurPool** (shown above), **StridedConv→ConvBlurPool**, and **AvgPool→BlurPool**.

et al., 2015; 2018; Yu & Koltun, 2016; Yu et al., 2017). This comes at great computation and memory cost. Our work investigates improving shift-equivariance with minimal additional computation, by blurring before subsampling.

Early networks employed average pooling (LeCun et al., 1990), which is equivalent to blurred-downsampling with a box filter. However, work (Scherer et al., 2010) has found max-pooling to be more effective, which has consequently become the predominant method for downsampling. While previous work (Scherer et al., 2010; Hénaff & Simoncelli, 2016; Azulay & Weiss, 2019) acknowledges the drawbacks of max-pooling and benefits of blurred-downsampling, they are viewed as separate, discrete choices, preventing their combination. Interestingly, Lee et al. (2016) does not explore low-pass filters, but does propose to softly gate between max and average pooling. However, this does not fully utilize the anti-aliasing capability of average pooling.

Mairal et al. (2014) derive a network architecture, motivated by translation invariance, named Convolutional Kernel Networks. While theoretically interesting (Bietti & Mairal, 2017), CKNs perform at lower accuracy than contemporaries, resulting in limited usage. Interestingly, a byproduct of the derivation is a standard Gaussian filter; however, no guidance is provided on its proper integration with existing network components. Instead, we demonstrate practical integration with any strided layer, and empirically show performance increases on a challenging benchmark – ImageNet

classification – on widely-used networks.

3. Methods

3.1. Preliminaries

Deep convolutional networks as feature extractors Let an image with resolution $H \times W$ be represented by $X \in \mathbb{R}^{H \times W \times 3}$. An L-layer CNN can be expressed as a feature extractor $\mathcal{F}_l(X) \in \mathbb{R}^{H_l \times W_l \times C_l}$, with layer $l \in [0, L]$, spatial resolution $H_l \times W_l$ and C_l channels. Each feature map can also be upsampled to original resolution, $\widetilde{\mathcal{F}}_l(X) \in \mathbb{R}^{H \times W \times C_l}$.

Shift-equivariance and invariance A function $\widetilde{\mathcal{F}}$ is shift-equivariant if shifting the input equally shifts the output, meaning shifting and feature extraction are commutable.

$$\text{Shift}_{\Delta h, \Delta w}(\widetilde{\mathcal{F}}(X)) = \widetilde{\mathcal{F}}(\text{Shift}_{\Delta h, \Delta w}(X)) \quad \forall (\Delta h, \Delta w) \tag{1}$$

A representation is shift-invariant if shifting the input results in an *identical* representation.

$$\widetilde{\mathcal{F}}(X) = \widetilde{\mathcal{F}}(\text{Shift}_{\Delta h, \Delta w}(X)) \quad \forall (\Delta h, \Delta w) \tag{2}$$

Periodic-N shift-equivariance/invariance In some cases, the definitions in Eqns. 1, 2 may hold only when shifts $(\Delta h, \Delta w)$ are integer multiples of N. We refer to such scenarios as periodic shift-equivariance/invariance. For example, periodic-2 shift-invariance means that even-pixel shifts
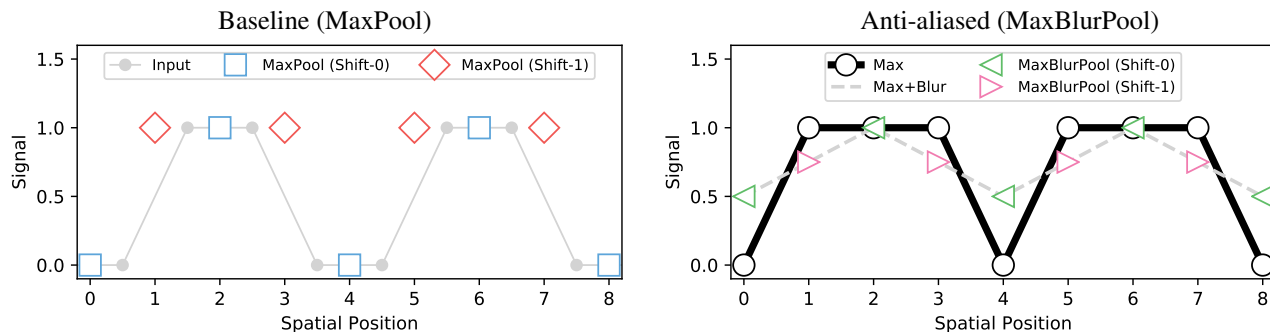
Figure 3. **Illustrative 1-D example of sensitivity to shifts.** We illustrate how downsampling affects shift-equivariance with a toy example. **(Left)** An input signal is in light gray line. Max-pooled ($k = 2$, $s = 2$) signal is in blue squares. Simply shifting the input and then max-pooling provides a completely different answer (red diamonds). **(Right)** The blue and red points are subsampled from a densely max-pooled ($k = 2$, $s = 1$) intermediate signal (**thick black line**). We low-pass filter this intermediate signal and then subsample from it, shown with green and magenta triangles, better preserving shift-equivariance.

produce an identical output, but odd-pixel shifts may not.

Circular convolution and shifting Edge artifacts are an important consideration. When an image is shifted, information is necessarily lost on one side and has to be filled in on the other.

In our CIFAR (Krizhevsky & Hinton, 2009) classification experiments, we use circular shifting and convolution. When the convolutional kernel hits the edge, it "rolls" to the other side. Similarly, when shifting, pixels are rolled off one edge to the other.

$$[\text{Shift}_{\Delta h, \Delta w}(X)]_{h,w,c} = X_{(h-\Delta h)\%H,(w-\Delta w)\%W,c} ,$$
$$\text{where } \% \text{ is the modulus function} \tag{3}$$

The modification minorly affects performance and could be potentially mitigated by additional padding, at the expense of memory and computation. But importantly, this affords us a clean testbed. Any loss in shift-equivariance or invariance is purely due to characteristics of the feature extractor.

An alternative approach is to take a shifted crop from a larger image. We use this approach for ImageNet (Russakovsky et al., 2015) experiments, as it more closely matches standard test procedures.

3.2. Anti-aliasing to improve shift-equivariance

Conventional methods for reducing spatial resolution – max-pooling, average pooling, and strided convolution – all break shift-equivariance. We start by analyzing max-pooling, the predominant downsampling method in deep networks.

MaxPool→MaxBlurPool Consider the example $[0, 0, 1, 1, 0, 0, 1, 1]$ signal in Fig. 3 (left). Max-pooling (kernel k=2, stride s=2) will result in $[0, 1, 0, 1]$. Simply shifting the input results in a dramatically different answer of $[1, 1, 1, 1]$. Shift-equivariance is lost. These

results are subsampling from an intermediate signal – the input densely max-pooled (stride-1), which we simply refer to as "max". As illustrated in Fig. 2 (top), we can write max-pooling as a composition of two functions: $\text{MaxPool}_{k,s} = \text{Subsample}_s \circ \text{Max}_k$.

The Max operation preserves shift-equivariance, as it is densely evaluated in a sliding window fashion, but subsequent subsampling does not. We simply propose to add an anti-aliasing filter with kernel $m \times m$, denoted as Blur_m as shown in Fig. 3 (right). During implementation, blurring and subsampling are combined, as commonplace in image processing. We call this function $\text{BlurPool}_{m,s}$.

$$\text{MaxPool}_{k,s} \rightarrow \text{Subsample}_s \circ \text{Blur}_m \circ \text{Max}_k$$
$$= \text{BlurPool}_{m,s} \circ \text{Max}_k \tag{4}$$

Sampling from the low-pass filtered signal gives $[.5, 1, .5, 1]$ and $[.75, .75, .75, .75]$. These are closer to each other and better representations of the intermediate signal.

StridedConv→ConvBlurPool Strided-convolutions suffer from the same issue, and the same method applies.

$$\text{Relu} \circ \text{Conv}_{k,s} \rightarrow \text{BlurPool}_{m,s} \circ \text{Relu} \circ \text{Conv}_{k,1} \tag{5}$$

Importantly, this analogous modification applies conceptually to any strided layer, meaning the network designer can keep their original operation of choice.

AveragePool→BlurPool Blurred downsampling with a box filter is the same as average pooling. Replacing it with a stronger filter provides better shift-equivariance. We examine such filters next.

$$\text{AvgPool}_{k,s} \rightarrow \text{BlurPool}_{m,s} \tag{6}$$

Anti-aliasing filter selection The method allows for a choice of blur kernel. We test filters ranging from size

| Method | Filter | VGG13-bn | | | |
| | | Train w/o aug | | Train w/ aug | |
		Acc	Con	Acc	Con
Baseline	**Delta-1**	91.6	88.1	**93.8**	96.6
Anti-Aliased	**Rect-2**	92.8	90.5	93.7	97.6
	Tri-3	93.1	93.9	93.6	98.0
	Bin-4	93.0	93.2	93.2	98.1
	Bin-5	**93.2**	96.3	93.2	98.4
	Bin-6	93.0	96.9	93.4	98.6
	Bin-7	93.0	**98.1**	93.2	**98.8**

Table 1. **CIFAR Classification.** We evaluate accuracy (Acc) and consistency (Con), using progressively larger anti-aliasing filters. We evaluate the network, training both without and with shift-based data augmentation. Results are plotted in Fig. 4.

2×2 to 7×7, with increasing smoothing. Weights are normalized to sum to 1.

- *Dirac Delta* (baseline) [1]: equivalent to subsampling and leaves the input unchanged
- *Rectangle-2* [1, 1]: often referred to as a moving average or box filter
- *Triangle-3* [1, 2, 1]: two box filters convolved together
- *Binomial-4, 5, 6, 7*: the box filter convolved with itself repeatedly. For example, *Bin-5* [1, 4, 6, 4, 1] is the standard filter used in Laplacian pyramids (Burt & Adelson, 1987).

4. Experiments

4.1. Testbeds

CIFAR Classification To begin, we test classification of low-resolution 32×32 images. The dataset contains 50k training and 10k validation images, classified into one of 10 categories. We dissect the VGG architecture (Simonyan & Zisserman, 2015), showing that shift-equivariance is a signal-processing property, progressively lost in each downsampling layer.

ImageNet Classification We then test on large-scale classification on 224×224 resolution images. The dataset contains 1.2M training and 50k validation images, classified into one of 1000 categories. We test across 4 different architectures – AlexNet (Krizhevsky & Hinton, 2009), VGG16 (Simonyan & Zisserman, 2015), ResNet50 (He et al., 2016), and DenseNet121 (Huang et al., 2017) – with different downsampling strategies, as described in Tab. 2.

Conditional Image Generation Finally, we show that the same aliasing issues in classification networks are also present in conditional image generation networks. We test on the Labels→Facades (Tyleček & Šára, 2013; Isola et al., 2017) dataset, where a network is tasked to generated a 256×256 photorealistic image from a label map. There are 400 training and 100 validation images.
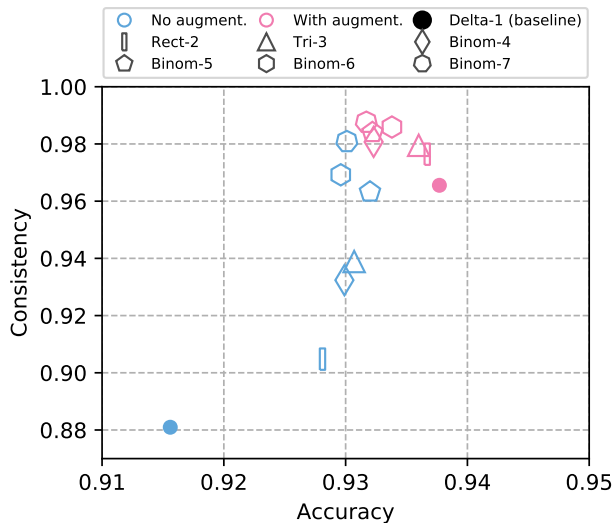

Figure 4. **CIFAR classification consistency vs accuracy.** Up (more consistent) and to the right (more accurate) is better. Number of sides corresponds to number of filter taps used (e.g., diamond for 4-tap filter); colors correspond to filters trained without (blue) and with (pink) shift-based data augmentation, using various filters. We show accuracy for no shift when training without shifts, and a random shift when training with shifts.

4.2. Shift-Invariance/Equivariance Metrics

Ideally, a shift in the input would result in equally shifted feature maps internally:

Internal feature distance. We examine internal feature maps with $d(\text{Shift}_{\Delta h, \Delta w}(\widetilde{\mathcal{F}}(X)), \widetilde{\mathcal{F}}(\text{Shift}_{\Delta h, \Delta w}(X)))$ (left & right-hand sides of Eqn. 1). We use cosine distance, as common for deep features (Kiros et al., 2015; Zhang et al., 2018).

We can also measure the stability of the output:

Classification consistency. For classification, we check how often the network outputs the same classification, given the same image with two different shifts: $\mathbb{E}_{X,h_1,w_1,h_2,w_2} \mathbb{1}\{\arg\max P(\text{Shift}_{h_1,w_1}(X)) = \arg\max P(\text{Shift}_{h_2,w_2}(X))\}$.

Generation stability. For image translation, we test if a shift in the input image generates a correspondingly shifted output. For simplicity, we test horizontal shifts. $\mathbb{E}_{X,\Delta w} \text{PSNR}(\text{Shift}_{0,\Delta w}(\mathcal{F}(X)), \mathcal{F}(\text{Shift}_{0,\Delta w}(X)))$.

4.3. Classification

4.3.1. CIFAR WITH VGG

We first test on the CIFAR dataset using the VGG13-bn (Simonyan & Zisserman, 2015) architecture. We train both without and with shift-based data augmentation. We evaluate on classification accuracy and consistency. The results are shown in Tab. 1 and Fig. 4.
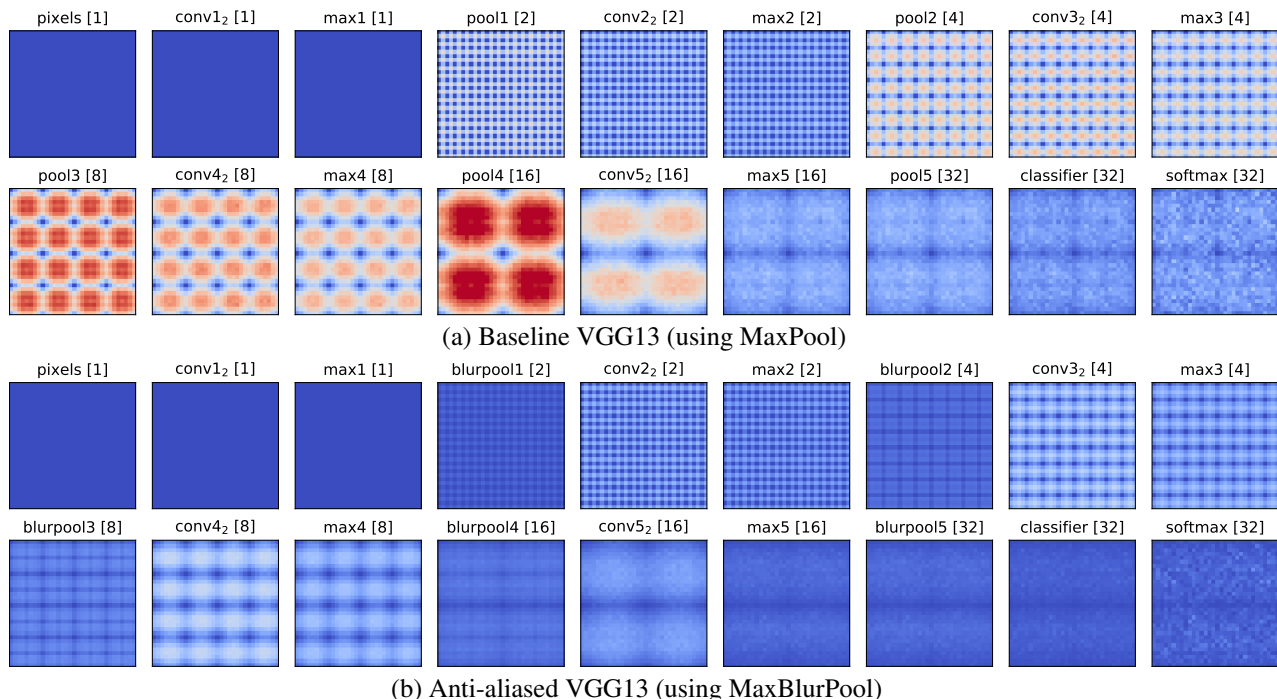
(a) Baseline VGG13 (using MaxPool)

(b) Anti-aliased VGG13 (using MaxBlurPool)

Figure 5. **Shift-equivariance throughout VGG.** Feature distance between left and right-hand sides of the shift-equivariance condition in Eqn 1. Each pixel in each heatmap is a shift $(\Delta h, \Delta w)$. Accumulated downsampling factor is in [brackets]; in the last three, shift-equivariance and shift-invariance are equivalent, as features have no spatial extent. Layers pix-max1 have perfect equivariance (0 at all shifts, shown by blue). **(a)** On the **baseline network**, shift-equivariance is reduced each time downsampling takes place. Periodic-N shift-equivariance holds, with N doubling with each downsampling. **(b)** With our **antialiased network**, shift-equivariance is better maintained, and the resulting output is more shift-invariant. The dynamic ranges of distances are different for each layer. For visualization, we calibrate by calculating the mean distance between two different images at a given layer, and mapping red to half the value.

Training without data augmentation Without the benefit of seeing shifts at training time, the baseline network produces inconsistent classifications – random shifts of the same image only agree 88.1% of the time. Our anti-aliased network, with the MaxBlurPool operator, increases consistency. The larger the filter, the more consistent the output classifications. This result agrees with our expectation and theory – improving shift-equivariance throughout the network should result in more consistent classifications across shifts, even when such shifts are not seen at training.

In this regime, accuracy clearly increases with consistency, as seen with the blue images in Fig. 4. Filtering does not destroy the signal or make learning harder. On the contrary, shift-equivariance serves as "built-in" augmentation, indicating more efficient data usage.

Training with data augmentation In principle, networks can *learn* to be shift-invariant from data. Is data augmentation all that is needed to achieve shift-invariance? By applying the *Rect-2* filter, a large increase in consistency, $96.6 \rightarrow 97.6$, can be had at a small decrease in accuracy $93.8 \rightarrow 93.7$. Even when seeing shifts at training, antialiasing increases consistency. From there, stronger filters can increase consistency, at the expense of accuracy.

Internal shift-equivariance We further dissect the progressive loss of shift-equivariance by investigating the VGG architecture internally. The network contains 5 blocks of convolutions, each followed by max-pooling (with stride 2), followed by a linear classifier. For purposes of our understanding, MaxPool layers are broken into two components – before and after subsampling, e.g., max1 and pool1, respectively. In Fig. 5 (top), we show internal feature distance, as a function of all possible shift-offsets $(\Delta h, \Delta w)$ and layers. All layers before the first downsampling, max1, are shift-equivariant. Once downsampling occurs in pool1, shift-equivariance is lost. However, periodic-N shift-equivariance still holds, as indicated by the stippling pattern in pool1, and each subsequent subsampling doubles the factor N.

In Fig. 5 (bottom), we plot shift-equivariance maps with our anti-aliased network, using MaxBlurPool. Shift-equivariance is clearly better preserved. In particular, the severe drop-offs in downsampling layers do not occur. Improved shift-equivariance throughout the network cascades into more consistent classifications in the output, as seen by some selected examples are in Fig. 1 (bottom). The plot is

	ImageNet Classification				Generation
	Alex-Net	VGG-16	Res-Net50	Dense-Net121	U-Net
StridedConv	1[†]	–	4[‡]	1[‡]	8
MaxPool	3	5	1	1	–
AvgPool	–	–	–	3	–

Table 2. **Testbeds.** We test across tasks (ImageNet classification and Labels→Facades) and network architectures. Each architecture employs different downsampling strategies. We list how often each is used here. We can antialias each variant. [†]The convolution uses stride 4 (all others use stride 2). We only apply the antialiasing at stride 2. Evaluating the convolution at stride 1 would require large computation at full-resolution. [‡]For the same reason, we do not antialias the first strided-convolution in these networks.

	ImageNet Classification							
	AlexNet		VGG16		ResNet50		DenseNet121	
Filter	Acc	Con	Acc	Con	Acc	Con	Acc	Con
Baseline	56.6	78.1	71.6	88.5	76.2	89.2	74.4	89.0
Rect-2	**57.2**	81.4	72.2	89.3	76.8	90.0	75.0	89.5
Tri-3	56.9	82.1	72.2	89.8	76.8	90.8	**75.1**	89.7
Bin-5	56.5	**82.5**	**72.3**	**90.2**	**77.0**	**91.6**	75.0	**90.3**

Table 3. **Imagenet Classification.** We show 1000-way classification accuracy and consistency (higher is better), across 4 architectures, with our anti-aliasing filtering added. We test 3 possible filters, in addition to the off-the-shelf reference models. As designed, classification consistency is improved across all methods. Interestingly, accuracy is *also improved*. We recommend *Tri-3* or *Bin-5* for general use.

made with a ***Bin-5*** filter, trained without data augmentation. The same trends hold for other filters and when training with augmentation.

Timing The average speed of a forward pass of VGG using batch size 100 CIFAR images on a GTX1080Ti GPU is 10.19ms. Evaluating Max at stride 1 instead of 2 adds 3.0%. From there, low-pass filtering with kernel sizes 3, 5, 7 adds additional $5.5\%, 7.6\%, 9.3\%$ time, respectively, relative to baseline. The method can be implemented more efficiently by separating the low-pass filter into horizontal and vertical components, allowing added time to scale linearly with filter size, rather than quadratically. In total, the largest filter adds 12.3% per forward pass. This is significantly cheaper than evaluating multiple forward passes in an ensembling approach ($1024\times$ computation to evaluate every shift), or evaluating each layer more densely by exchanging striding for dilation ($4\times, 16\times, 64\times, 256\times$ computation for `conv2-conv5`, respectively). Given computational resources, brute-force computation solves shift-invariance.

Additional analysis We present additional analysis in the supplementary material – using DenseNet (Huang et al., 2017), investigating how learned convolutional layers change in an anti-aliased net, swapping Max and Blur operations, combining Max and Blur in parallel rather than
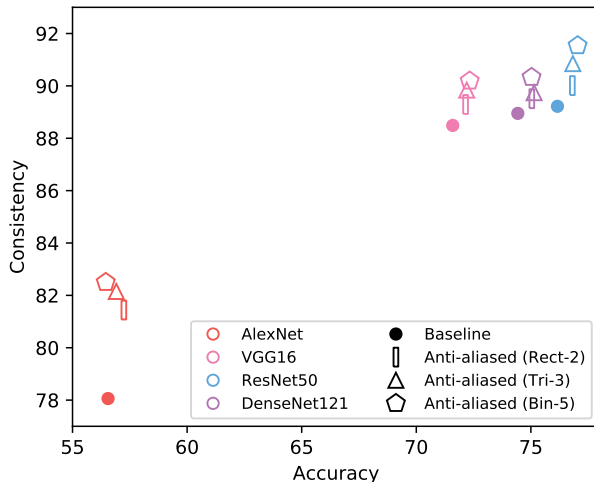

Figure 6. **ImageNet Classification consistency vs. accuracy.** Up (more consistent) and to the right (more accurate) is better. Different colors correspond to different networks, and different shapes correspond to the baseline (circle) or variants of our anti-aliased networks (bar, triangle, pentagon for length 2, 3, 5 filters). As expected, low-pass filtering helps shift-invariance. Surprisingly, classification accuracy is also improved.

in series, a negative result on learning the blur filter, and robustness against a shift-based adversarial attacker.

4.3.2. LARGE-SCALE IMAGENET CLASSIFICATION

We next test on large-scale image classification of ImageNet (Russakovsky et al., 2015). In Tab. 3, we show classification accuracy and consistency, across several architectures – AlexNet, VGG16, Resnet50, and DenseNet121. The off-the-shelf networks, are labeled as "baseline", and we use standard training schedules from the publicly available PyTorch (Paszke et al., 2017) repository for our anti-aliased networks. Each architecture has a different downsampling strategy, shown in Tab. 2. For example, VGG exclusively uses MaxPooling, whereas DenseNet uses a StridedConv, a MaxPool, and 3 AvgPools. The consistency and accuracy of baseline and anti-aliased networks are visualized in Fig. 6.

Improved shift-invariance We apply progressively stronger filters – *Rect-2, Tri-3, Bin-5* – to the 4 architectures. Using a small *Rect-2* filter increases consistency by +3.39, +0.80, +0.79, and +0.56%, across AlexNet, VGG, ResNet, and DenseNet, respectively. The *Bin-5* filter increases by +4.44, +1.70, +2.32, and +1.38%. As expected, the larger the filter, the more shift-invariant the output.

Classification performance Filtering improves the shift-invariance. How does it affect absolute classification performance? We find that across the board, *performance actually modestly increases*. A *Rect-2* filter increases AlexNet by +0.69%. *Bin-5* increases VGG16 and Resnet to +0.74% and +0.88%, respectively. *Tri-3* increases DenseNet by +0.72%.
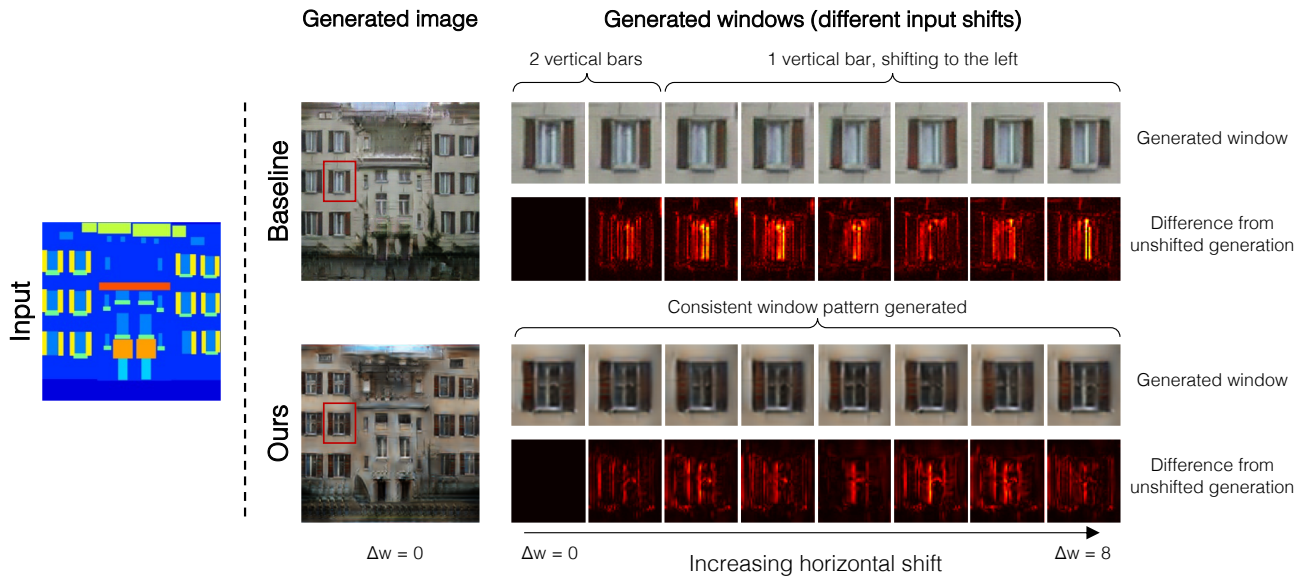
Figure 7. **Selected example of generation instability.** The left two images are generated facades from label maps. For the baseline method (top), input shifts cause different window patterns to emerge, due to naive downsampling and upsampling. Our method (bottom) stabilizes the output, generating the same window pattern, regardless the input shift.

While certain filters work better for certain networks, of the 12 combinations of filters and networks we examined, 11 improve accuracy (all improve consistency). This is a surprising, unexpected result, as low-pass filtering removes information, and could be expected to reduce performance. On the contrary, we find that it serves as effective regularization, and these widely-used methods improve with simple anti-aliasing. As ImageNet-trained nets often serve as the backbone for downstream tuning, this potential improvement may be observed across other applications as well.

We recommend using the *Tri-3* or *Bin-5* filter. If shift-invariance is especially desired, stronger filters can be used.

4.4. Conditional image generation (Label→Facades)

We test on image generation, outputting an image of a facade given its semantic label map (Tyleček & Šára, 2013).

Baseline We use the pix2pix method (Isola et al., 2017). The method uses U-Net (Ronneberger et al., 2015), which contains 8 downsampling and 8 upsampling layers, with skip connections to preserve local information. No anti-aliasing filtering is applied in down or upsampling layers in the baseline. In Fig. 7, we show a qualitative example, focusing in on a specific window. In the baseline (top), as the input X shifts horizontally by Δw, the vertical bars on the generated window also shift. The generations start with two bars, to a single bar, and eventually oscillates back to two bars. A shift-equivariant network would provide the same resulting facade, no matter the shift.

Applying anti-aliasing filtering We augment the strided-

	Delta-1	Rect-2	Tri-3	Bin-4	Bin-5
Stability [dB]	29.0	30.1	30.8	31.2	34.4
TV Norm $\times 100$	7.48	7.07	6.25	5.84	6.28

Table 4. **Generation stability** PSNR (higher is better) between generated facades, given two horizontally shifted inputs. More aggressive filtering in the down and upsampling layers leads to a more shift-equivariant generator. **Total variation (TV) of generated images** (closer to ground truth images 7.80 is better). Increased filtering decreases the frequency content of generated images.

convolution downsampling by blurring. The U-Net also uses upsampling layers, without any smoothing. Similar to the subsampling case, this leads to aliasing, in the form of grid artifacts (Odena et al., 2016). We mirror the downsampling by applying the same filter after upsampling. Note that applying the *Rect-2* and *Tri-3* filters while upsampling correspond to "nearest" and "bilinear" upsampling, respectively. By using the *Tri-3* filter, the same window pattern is generated, regardless of input shift, as seen in Fig. 7 (bot).

We measure similarity using peak signal-to-noise ratio between generated facades with shifted and non-shifted inputs: $\mathbb{E}_{X,\Delta w}\text{PSNR}(\text{Shift}_{0,\Delta w}(F(X)), F(\text{Shift}_{0,\Delta w}(X))))$. In Tab. 4, we show that the smoother the filter, the more shift-equivariant the output.

A concern with adding low-pass filtering is the loss of ability to generate high-frequency content, which is critical for generating high-quality imagery. Quantitatively, in Tab. 4, we compute the total variation (TV) norm of the generated images. Qualitatively, we observe that generation quality typically holds with the *Tri-3* filter and subsequently de-

grades. In the supplemental material, we show examples of applying increasingly aggressive filters. We observe a boost in shift-equivariance while maintaining generation quality, and then a tradeoff between the two factors.

These experiments demonstrate that the technique can make a drastically different architecture (U-Net) for a different task (generating pixels) more shift-equivariant.

5. Conclusions and Discussion

In summary, we show that shift-invariance is lost in modern deep networks, as commonly used pooling layers ignore Nyquist sampling and alias. We integrate low-pass filtering to anti-alias, a common signal processing technique, as a simple architectural modification. Our integration allows the network architecture designer to keep their pooling layer of choice but still anti-alias the network. We achieve higher consistency in both image classification and conditional image generation scenarios, across different architectures and downsampling techniques.

In addition, we show large improvements in both performance and consistency when training without data augmentation. This is potentially applicable to online learning scenarios, where the data distribution is changing. In large-scale ImageNet classification, we observe a modest boost in classification, across architectures, even when training with data augmentation. Future directions include exploring the potential benefit to downstream applications, such as nearest-neighbor retrieval, improving temporal consistency in video models, robustness to adversarial examples, and high-level vision tasks such as detection.

CHANGELOG

v1 ArXiv preprint. Paper accepted to ICML 2019.

References

Adelson, E. H., Anderson, C. H., Bergen, J. R., Burt, P. J., and Ogden, J. M. Pyramid methods in image processing. *RCA engineer*, 29(6):33–41, 1984.

Aubry, M. and Russell, B. C. Understanding deep features with computer-generated imagery. In *ICCV*, 2015.

Azulay, A. and Weiss, Y. Why do deep convolutional networks generalize so poorly to small image transformations? In *arXiv*, 2019.

Bietti, A. and Mairal, J. Invariance and stability of deep convolutional representations. In *NIPS*, 2017.

Bruna, J. and Mallat, S. Invariant scattering convolution networks. *TPAMI*, 2013.

Burt, P. J. and Adelson, E. H. The laplacian pyramid as a compact image code. In *Readings in Computer Vision*, pp. 671–679. Elsevier, 1987.

Chen, L.-C., Papandreou, G., Kokkinos, I., Murphy, K., and Yuille, A. L. Semantic image segmentation with deep convolutional nets and fully connected crfs. In *ICLR*, 2015.

Chen, L.-C., Papandreou, G., Kokkinos, I., Murphy, K., and Yuille, A. L. Deeplab: Semantic image segmentation with deep convolutional nets, atrous convolution, and fully connected crfs. *TPAMI*, 2018.

Cohen, T. and Welling, M. Group equivariant convolutional networks. In *ICML*, 2016.

Dosovitskiy, A. and Brox, T. Generating images with perceptual similarity metrics based on deep networks. In *NIPS*, 2016a.

Dosovitskiy, A. and Brox, T. Inverting visual representations with convolutional networks. In *CVPR*, 2016b.

Engstrom, L., Tsipras, D., Schmidt, L., and Madry, A. A rotation and a translation suffice: Fooling cnns with simple transformations. In *arXiv*, 2017.

Esteves, C., Allen-Blanchette, C., Zhou, X., and Daniilidis, K. Polar transformer networks. In *ICLR*, 2018.

Fawzi, A. and Frossard, P. Manitest: Are classifiers really invariant? In *BMVC*, 2015.

Foley, J. D., van Dam, A., Feiner, S. K., and Hughes, J. F. *Computer Graphics: Principles and Practice*. Addison-Wesley, 2nd edition, 1995.

Fowler, J. E. The redundant discrete wavelet transform and additive noise. *IEEE Signal Processing Letters*, 12(9): 629–632, 2005.

Fukushima, K. and Miyake, S. Neocognitron: A self-organizing neural network model for a mechanism of visual pattern recognition. In *Competition and cooperation in neural nets*, pp. 267–285. Springer, 1982.

Girshick, R., Donahue, J., Darrell, T., and Malik, J. Rich feature hierarchies for accurate object detection and semantic segmentation. In *CVPR*, 2014.

Gonzalez, R. C. and Woods, R. E. *Digital Image Processing*. Pearson, 2nd edition, 1992.

Goodfellow, I., Lee, H., Le, Q. V., Saxe, A., and Ng, A. Y. Measuring invariances in deep networks. In *NIPS*, 2009.

Goodfellow, I., Pouget-Abadie, J., Mirza, M., Xu, B., Warde-Farley, D., Ozair, S., Courville, A., and Bengio, Y. Generative adversarial nets. In *NIPS*, 2014a.

Goodfellow, I. J., Shlens, J., and Szegedy, C. Explaining and harnessing adversarial examples. *ICLR*, 2014b.

He, K., Zhang, X., Ren, S., and Sun, J. Deep residual learning for image recognition. In *CVPR*, 2016.

Hénaff, O. J. and Simoncelli, E. P. Geodesics of learned representations. In *ICLR*, 2016.

Huang, G., Liu, Z., Van Der Maaten, L., and Weinberger, K. Q. Densely connected convolutional networks. In *CVPR*, 2017.

Hubel, D. H. and Wiesel, T. N. Receptive fields, binocular interaction and functional architecture in the cat's visual cortex. *The Journal of physiology*, 160(1):106–154, 1962.

Isola, P., Zhu, J.-Y., Zhou, T., and Efros, A. A. Image-to-image translation with conditional adversarial networks. In *CVPR*, 2017.

Kanazawa, A., Sharma, A., and Jacobs, D. Locally scale-invariant convolutional neural networks. In *NIPS Workshop*, 2014.

Kiros, R., Zhu, Y., Salakhutdinov, R. R., Zemel, R., Urtasun, R., Torralba, A., and Fidler, S. Skip-thought vectors. In *NIPS*, 2015.

Krizhevsky, A. and Hinton, G. Learning multiple layers of features from tiny images. Technical report, Citeseer, 2009.

Krizhevsky, A., Sutskever, I., and Hinton, G. E. Imagenet classification with deep convolutional neural networks. In *NIPS*, 2012.

LeCun, Y., Boser, B. E., Denker, J. S., Henderson, D., Howard, R. E., Hubbard, W. E., and Jackel, L. D. Handwritten digit recognition with a back-propagation network. In *NIPS*, 1990.

LeCun, Y., Bottou, L., Bengio, Y., and Haffner, P. Gradient-based learning applied to document recognition. *Proceedings of the IEEE*, 86(11):2278–2324, 1998.

Lee, C.-Y., Gallagher, P. W., and Tu, Z. Generalizing pooling functions in convolutional neural networks: Mixed, gated, and tree. In *AIStats*, 2016.

Lenc, K. and Vedaldi, A. Understanding image representations by measuring their equivariance and equivalence. In *CVPR*, 2015.

Leung, T. and Malik, J. Representing and recognizing the visual appearance of materials using three-dimensional textons. *IJCV*, 2001.

Lowe, D. G. Object recognition from local scale-invariant features. In *ICCV*, 1999.

Mahendran, A. and Vedaldi, A. Understanding deep image representations by inverting them. In *CVPR*, 2015.

Mairal, J., Koniusz, P., Harchaoui, Z., and Schmid, C. Convolutional kernel networks. In *NIPS*, 2014.

Mordvintsev, A., Olah, C., and Tyka, M. Deepdream-a code example for visualizing neural networks. *Google Research*, 2:5, 2015.

Nguyen, A., Clune, J., Bengio, Y., Dosovitskiy, A., and Yosinski, J. Plug & play generative networks: Conditional iterative generation of images in latent space. In *CVPR*, 2017.

Nyquist, H. Certain topics in telegraph transmission theory. *Transactions of the American Institute of Electrical Engineers*, pp. 617–644, 1928.

Odena, A., Dumoulin, V., and Olah, C. Deconvolution and checkerboard artifacts. *Distill*, 2016. doi: 10.23915/distill.00003. URL http://distill.pub/2016/deconv-checkerboard.

Oppenheim, A. V., Schafer, R. W., and Buck, J. R. *Discrete-Time Signal Processing*. Pearson, 2nd edition, 1999.

Paszke, A., Gross, S., Chintala, S., Chanan, G., Yang, E., DeVito, Z., Lin, Z., Desmaison, A., Antiga, L., and Lerer, A. Automatic differentiation in pytorch. 2017.

Ronneberger, O., Fischer, P., and Brox, T. U-net: Convolutional networks for biomedical image segmentation. In *MICCAI*, 2015.

Ruderman, A., Rabinowitz, N. C., Morcos, A. S., and Zoran, D. Pooling is neither necessary nor sufficient for appropriate deformation stability in cnns. In *arXiv*, 2018.

Russakovsky, O., Deng, J., Su, H., Krause, J., Satheesh, S., Ma, S., Huang, Z., Karpathy, A., Khosla, A., Bernstein, M., et al. Imagenet large scale visual recognition challenge. *IJCV*, 115(3):211–252, 2015.

Scherer, D., Muller, A., and Behnke, S. Evaluation of pooling operations in convolutional architectures for object recognition. In *ICANN*. 2010.

Sifre, L. and Mallat, S. Rotation, scaling and deformation invariant scattering for texture discrimination. In *CVPR*, 2013.

Simoncelli, E. P., Freeman, W. T., Adelson, E. H., and Heeger, D. J. Shiftable multiscale transforms. *IEEE transactions on Information Theory*, 38(2):587–607, 1992.

Simonyan, K. and Zisserman, A. Very deep convolutional networks for large-scale image recognition. In *ICLR*, 2015.

Su, J., Vargas, D. V., and Sakurai, K. One pixel attack for fooling deep neural networks. *IEEE Transactions on Evolutionary Computation*, 2019.

Szeliski, R. *Computer vision: algorithms and applications*. Springer Science & Business Media, 2010.

Tyleček, R. and Šára, R. Spatial pattern templates for recognition of objects with regular structure. In *German Conference on Pattern Recognition*, pp. 364–374. Springer, 2013.

Vedaldi, A. and Fulkerson, B. VLFeat: An open and portable library of computer vision algorithms. http://www.vlfeat.org/, 2008.

Worrall, D. E., Garbin, S. J., Turmukhambetov, D., and Brostow, G. J. Harmonic networks: Deep translation and rotation equivariance. In *CVPR*, 2017.

Xiao, C., Zhu, J.-Y., Li, B., He, W., Liu, M., and Song, D. Spatially transformed adversarial examples. *ICLR*, 2018.

Yu, D., Wang, H., Chen, P., and Wei, Z. Mixed pooling for convolutional neural networks. In *International Conference on Rough Sets and Knowledge Technology*, pp. 364–375. Springer, 2014.

Yu, F. and Koltun, V. Multi-scale context aggregation by dilated convolutions. *ICLR*, 2016.

Yu, F., Koltun, V., and Funkhouser, T. Dilated residual networks. In *CVPR*, 2017.

Zeiler, M. D. and Fergus, R. Visualizing and understanding convolutional networks. In *ECCV*, 2014.

Zhang, R., Isola, P., Efros, A. A., Shechtman, E., and Wang, O. The unreasonable effectiveness of deep features as a perceptual metric. In *CVPR*, 2018.

Zhou, B., Khosla, A., Lapedriza, A., Oliva, A., and Torralba, A. Object detectors emerge in deep scene cnns. In *ICLR*, 2015.

Supplementary Material

A. CIFAR Classification Analysis

In the main paper, we presented results on the older VGG (Simonyan & Zisserman, 2015) network. Here, we also present results using a variant of the more modern DenseNet (Huang et al., 2017) architecture.

Architecture	Classification (CIFAR)	
	VGG13-bn	DenseNet-40-12
StridedConv	–	–
MaxPool	5	–
AvgPool	–	2

Table 5. **Testbeds (CIFAR10 Architectures).** We use slightly different architectures for VGG (Simonyan & Zisserman, 2015) and DenseNet (Huang et al., 2017) than the ImageNet counterparts.

A.1. DenseNet results

We show a summary of VGG and DenseNet in Tab. 5. This supplements Tab. 2 in the main paper. DenseNet uses comparatively fewer downsampling layers – 2 average-pooling layers instead of 5 max-pooling layers. With just two downsampling layers, the baseline still loses shift-invariance. Even when training with data augmentation, replacing average-pooling with blurred-pooling increases both consistency and even minorly improves accuracy. Note that the DenseNet architecture performs stronger than VGG to begin with. In this setting, the *Bin-7* BlurPool operator works best for both consistency and accuracy. Again, applying the operator serves are "built-in" data augmentation, performing strongly even without shifts at train time.

A.2. How do the learned convolutional filters change?

Our proposed change smooths the internal feature maps for purposes of downsampling. How does training with this layer affect the *learned* convolutional layers? We measure spatial smoothness using the normalized Total Variation (TV) metric proposed in Ruderman et al. (2018). A higher value indicates a filter with more high-frequency components. A lower value indicates a smoother filter. As shown in Fig. 10, the anti-aliased networks (red-purple) actually learn smoother filters throughout the network, relative to the baseline (black). Adding in more aggressive low-pass filtering further decreases the TV (increasing smoothness). This indicates that our method actually induces a smoother feature extractor overall.

A.3. Average accuracy across spatial positions

In Fig. 9, we train without augmentation, and show how accuracy systematically degrades as a function of spatial

Net	Filter shape	# Taps	Weights	Train w/o augmentation			Train w/ augmentation		
				Accuracy		Consistency	Accuracy		Consistency
				None	Rand		None	Rand	
	Delta (baseline)	1	[1]	91.6	87.4	88.1	93.4	**93.8**	96.6
	Rectangle	2	[1, 1]	92.8	89.3	90.5	**93.9**	93.7	97.6
	Triangle	3	[1, 2, 1]	93.1	91.4	93.9	93.6	93.6	98.0
VGG	**Binomial**	4	[1, 3, 3, 1]	93.0	91.1	93.2	93.4	93.2	98.1
	Binomial	5	[1, 4, 6, 4, 1]	**93.2**	92.6	96.3	93.1	93.2	98.4
	Binomial	6	[1, 5, 10, 10, 5, 1]	93.0	92.4	96.9	93.4	93.4	98.6
	Binomial	7	[1, 6, 15, 20, 15, 6, 1]	93.0	**93.0**	**98.1**	93.2	93.2	**98.8**
	Delta	1	[1]	92.0	89.9	91.5	93.9	93.9	97.3
	Rect (baseline)	2	[1, 1]	93.0	92.3	94.8	94.4	94.4	97.7
Dense	**Triangle**	3	[1, 2, 1]	93.9	93.5	96.7	**94.5**	94.5	98.3
	Binomial	5	[1, 4, 6, 4, 1]	94.4	94.0	98.1	**94.5**	94.5	98.8
	Binomial	7	[1, 6, 15, 20, 15, 6, 1]	**94.5**	**94.3**	**98.8**	**94.5**	94.6	**98.9**

Table 6. **CIFAR Classification accuracy and consistency, with DenseNet.** The VGG results have been shown in Tab. 1 and are included here for completeness. We show DenseNet results here as well. Results across blurring filters and training scenarios (without and with data augmentation). We evaluate classification accuracy without shifts (**Accuracy – None**) and on random shifts (**Accuracy – Random**), as well as classification **consistency**.
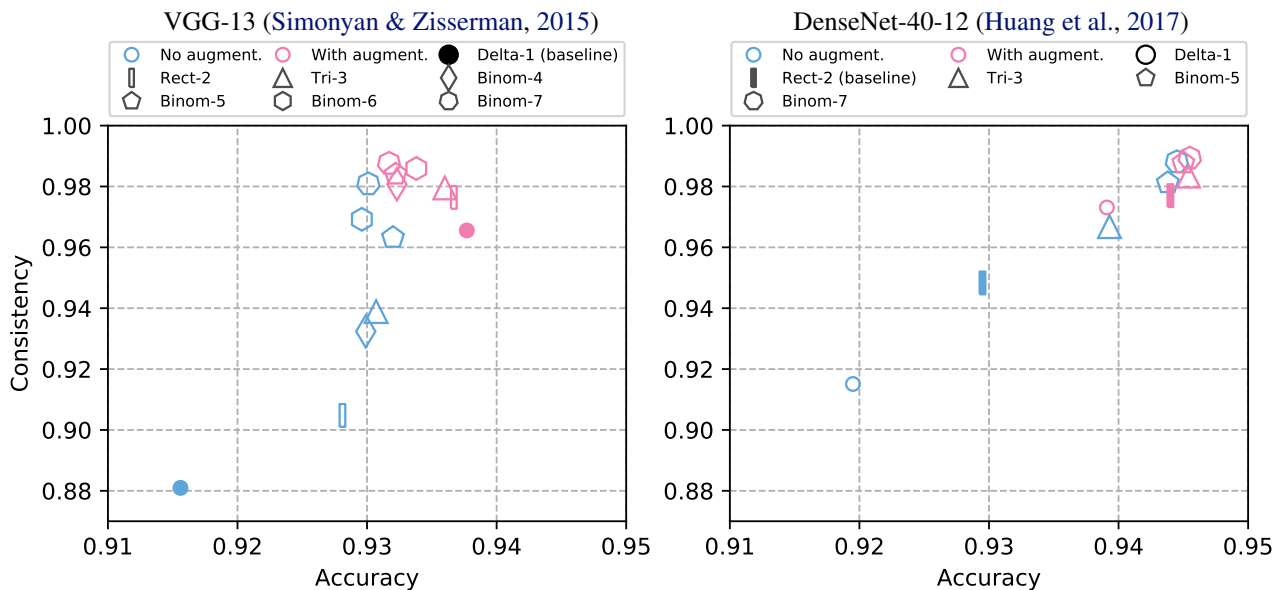

Figure 8. **CIFAR10 Classification consistency vs. accuracy.** VGG (**left**) and DenseNet (**right**) networks. Up (more consistent) and to the right (more accurate) is better. Number of sides corresponds to number of filter taps used (e.g., diamond for 4-tap filter); colors correspond to filters trained without (blue) and with (pink) shift-based data augmentation, using various filters. We show accuracy for no shift when training without shifts, and a random shift when training with shifts.
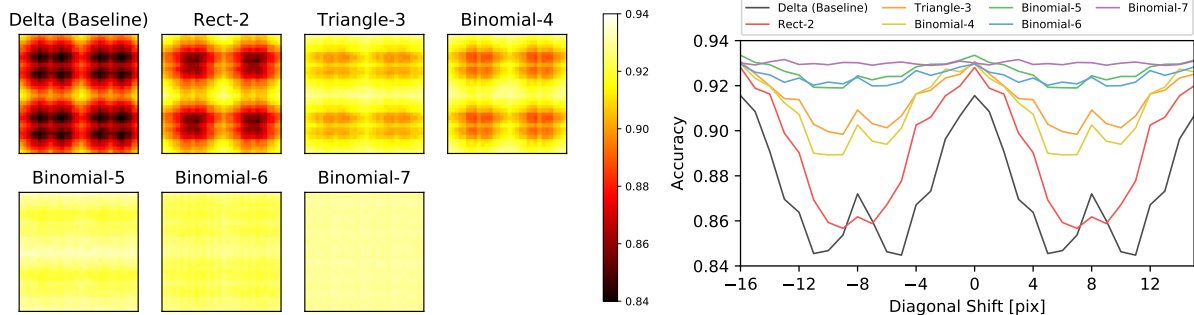
Figure 9. **Average accuracy as a function of shift. (Left)** We show classification accuracy across the test set as a function of shift, given different filters. **(Right)** We plot accuracy vs diagonal shift in the input image, across different filters. Note that accuracy degrades quickly with the baseline, but as increased filtering is added, classifications become consistent across spatial positions.
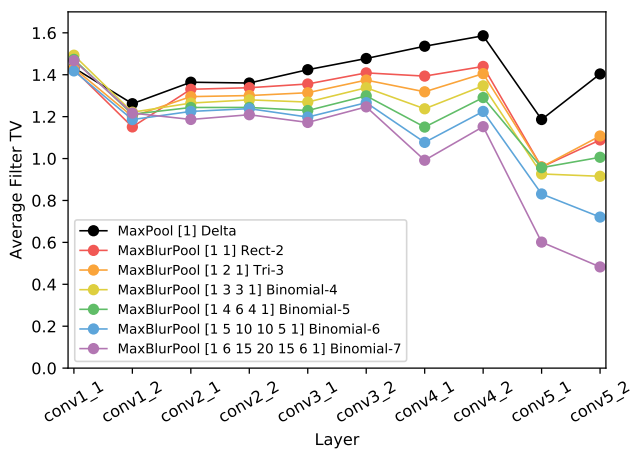

Figure 10. **Total Variation (TV) by layer.** We compute average smoothness of learned conv filters per layer (lower is smoother). Baseline MaxPool is in black, and adding additional blurring is shown in colors. Note that the *learned* convolutional layers become smoother, indicating that a smoother feature extractor is induced.

shift. We observe the following:

- On the left, the baseline heatmap shows that classification accuracy holds when testing with no shift, but quickly degrades when shifting.
- The proposed filtering decreases the degradation. *Bin-7* is largely consistent across all spatial positions.
- On the right, we plot the accuracy when making diagonal shifts to the input. As increased filtering is added, classification accuracy becomes consistent in all positions.

A.4. Classification variation distribution

The consistency metric in the main paper looks at the hard classification, discounting classifier confidence. Similar to Azulay & Weiss (2019), we also compute the variation in probability of correct classification (the traces shown in Fig. 2 in the main paper), given different shifts.

We can capture the variation across all possible shifts:
$$\sqrt{Var_{h,w}(\{P_{\text{correct class}}(\text{Shift}_{h,w}(X))\})}.$$

In Fig. 11, we show the distribution of classification variations, before and after adding in the low-pass filter. Even with a small 2×2 filter, immediately variation decreases. As the filter size is increased, the output classification variation continues to decrease. This has a larger effect when training without data augmentation, but is still observable when training with data augmentation.

Training with data augmentation with the baseline network reduces variation. Anti-aliasing the networks reduces variation in both scenarios. More aggressive filtering further decreases variation.

A.5. Robustness to shift-based adversary

In the main paper, we show that anti-aliased the networks increases the classification consistency, while maintaining accuracy. A logical consequence is increased accuracy in presence of a shift-based adversary. We empirically confirm this in Fig. 12 for VGG13 on CIFAR10. We compute classification accuracy as a function of maximum adversarial shift. A max shift of 2 means the adversary can choose any of the 25 positions within a 5×5 window. For the classifier to "win", it must correctly classify all of them correctly. Max shift of 0 means that there is no adversary. Conversely, a max shift of 16 means the image must be correctly classified at all $32 \times 32 = 1024$ positions.

Our primary observations are as follows:

- As seen in Fig. 12 (left), the baseline network (gray) is very sensitive to the adversary.
- Adding larger *Binomial* filters (from red to purple) increases robustness to the adversary. In fact, *Bin-7* filter (purple) *without* augmentation outperforms the baseline (black) *with* augmentation.
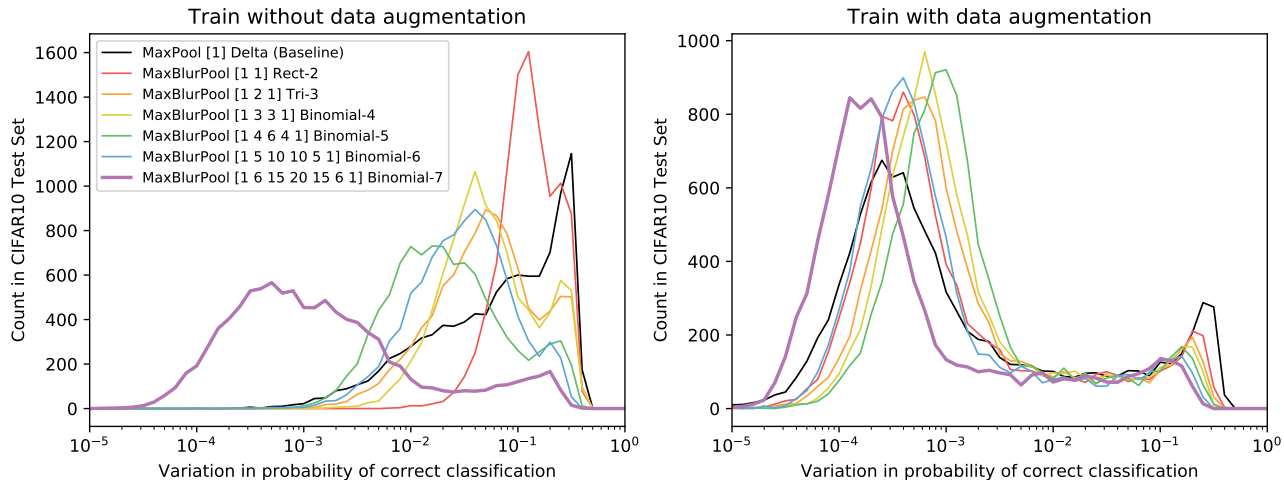- As seen in Fig. 12 (right), adding larger *Binomial* filters

Figure 11. **Distribution of per-image classification variation.** We show the distribution of classification variation in the test set, **(left)** without and **(right)** with data augmentation at training. Lower variation means more consistent classifications (and increased shift-invariance). Training with data augmentation drastically reduces variation in classification. Adding filtering further decreases variation.

also increases adversarial robustness, even when training with augmentation.

These results corroborate the findings in the main paper, and demonstrate a use case: increased robustness to a shift-based adversarial attack.

B. Alternatives to MaxBlurPool

In the paper, we follow signal processing first principles, to arrive at our solution of MaxBlurPool, with a fixed blurring kernel. Here, we explore possible alternatives – swapping max and blur operations, combining max and blur in parallel through soft-gating, and learning the blur filter.

B.1. Swapping max and blur

We blur after max, immediately before subsampling, which has solid theoretical backing in sampling theory. What happens when the operations are swapped? The signal before the max operator is undoubtedly related to the signal after. Thus, blurring before max provides "second-hand" anti-aliasing and still increases shift-invariance over the baseline. However, switching the order is worse than max and blurring in the correct, proposed order. For example, for *Bin-7*, accuracy ($93.2 \rightarrow 92.6$) and consistency ($98.8 \rightarrow 98.6$) both decrease. We consistently observe this across filters.

B.2. Softly gating between max-pool and average-pool

Lee et al. (2016) investigate combining MaxPool and Avg-Pool in parallel, with a soft-gating mechanism, called "Mixed" Max-AvgPool. We instead combine them in series. We conduct additional experiments here. On CIFAR (VGG

w/ aug, see Tab 6), MixedPool can offer improvements over MaxPool baseline ($96.6 \rightarrow 97.2$ consistency). However, by softly weighting AvgPool, some antialiasing capability is left on the table. MaxBlurPool provides higher invariance (97.6). All have similar accuracy – 93.8, 93.7, and 93.7 for baseline MaxPool, MixedPool, and our MaxBlurPool, respectively. We use our *Rect-2* variant here for clean comparison.

Importantly, our paper proposes a methodology, not a pooling layer. The same technique to modify MaxPool (reduce stride, then BlurPool) applies to the MixedPool layer, increasing its shift-invariance ($97.2 \rightarrow 97.8$).

B.3. Learning the blur filter

We have shown that adding anti-aliasing filtering improves shift-equivariance. What if the blur kernel were learned? We initialize the filters with our fixed weights, *Tri-3* and *Bin-5*, and allow them to be adjusted during training (while constraining the kernel symmetrical). The function space has more degrees of freedom and is strictly more general. However, we find that while accuracy holds, consistency decreases: relative to the fixed filters, we see $98.0 \rightarrow 97.5$ for length-3 and $98.4 \rightarrow 97.3$ for length-5. While shift-invariance *can* be learned, there is no explicit incentive to do so. Analogously, a fully connected network *can* learn convolution, but does not do so in practice.

C. ImageNet Classification

We show expanded results and visualizations. In Tab. 7, we show expanded results. This contains the same results as in Tab. 3, but with Δ performance between our method and the baseline shown. In Fig. 13, we show all 4 architectures,
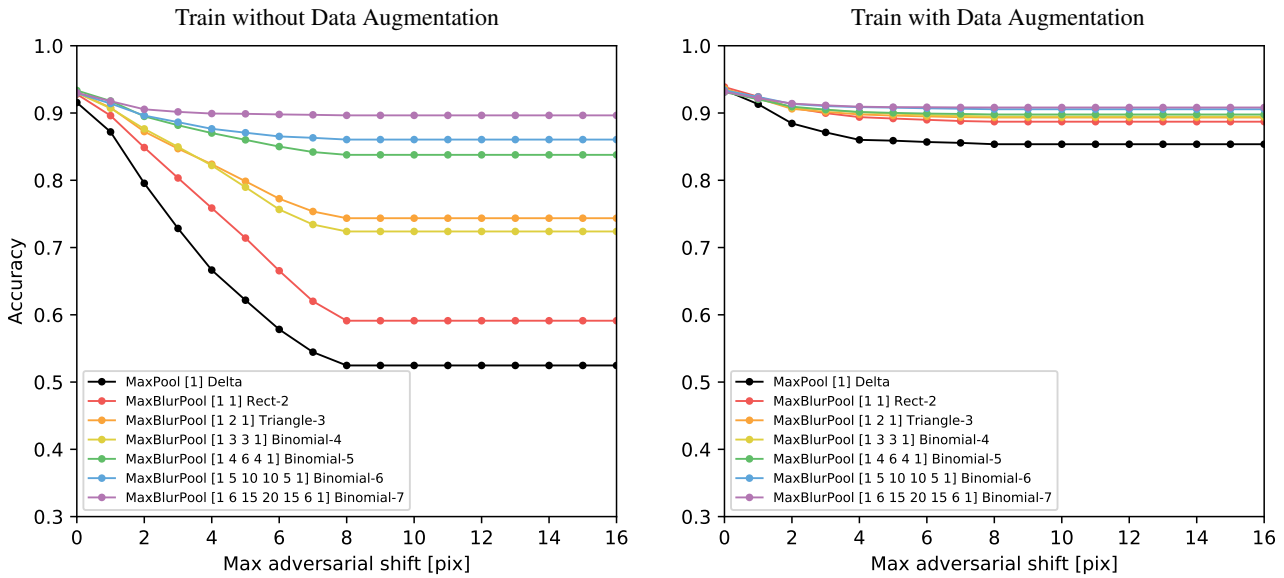
Figure 12. **Robustness to shift-based adversarial attack.** Classification accuracy as a function of the number of pixels an adversary is allowed to shift the image. Applying our proposed filtering increases robustness, both without **(left)** and with **right** data augmentation.

with each of the 3 filters tested.

D. Qualitative examples for Labels→Facades

In the main paper, we discussed the tension between needing to generate high-frequency content and low-pass filtering for shift-invariance. Here, we show an example of applying increasingly aggressive filters. In general, generation quality is maintained with the *Rect-2* and *Tri-3* filters, and then degrades with additional filtering.

	AlexNet (Krizhevsky et al., 2012)				VGG16 (Simonyan & Zisserman, 2015)				ResNet50 (He et al., 2016)				DenseNet121 (Huang et al., 2017)			
	Accuracy		Consistency		Accuracy		Consistency		Accuracy		Consistency		Accuracy		Consistency	
Filter	Abs	Δ	Abs	Δ	Abs	Δ	Abs	Δ	Abs	Δ	Abs	Δ	Abs	Δ	Abs	Δ
Baseline	56.55	–	78.06	–	71.59	–	88.49	–	76.16	–	89.22	–	74.43	–	88.95	–
Rect-2	**57.24**	**+0.69**	81.44	+3.39	72.15	+0.56	89.29	+0.80	76.81	+0.66	90.01	+0.79	75.04	+0.61	89.51	+0.56
Tri-3	56.91	+0.35	82.15	+4.10	72.20	+0.61	89.84	+1.36	76.83	+0.67	90.85	+1.63	**75.14**	**+0.72**	89.74	+0.79
Bin-5	56.45	-0.10	**82.50**	**+4.44**	**72.33**	**+0.74**	**90.19**	**+1.70**	**77.04**	**+0.88**	**91.54**	**+2.32**	75.03	+0.60	**90.33**	**+1.38**

Table 7. **Imagenet Classification.** We show 1000-way classification accuracy and consistency (higher is better), across 4 architectures, with anti-aliasing filtering added. We test 3 possible filters, in addition to the off-the-shelf reference models. This is an expanded version of Table 3 in the main paper. **Abs** is the absolute performance, and Δ is the difference to the baseline. As designed, classification consistency is improved across all methods. Interestingly, accuracy is *also improved*.
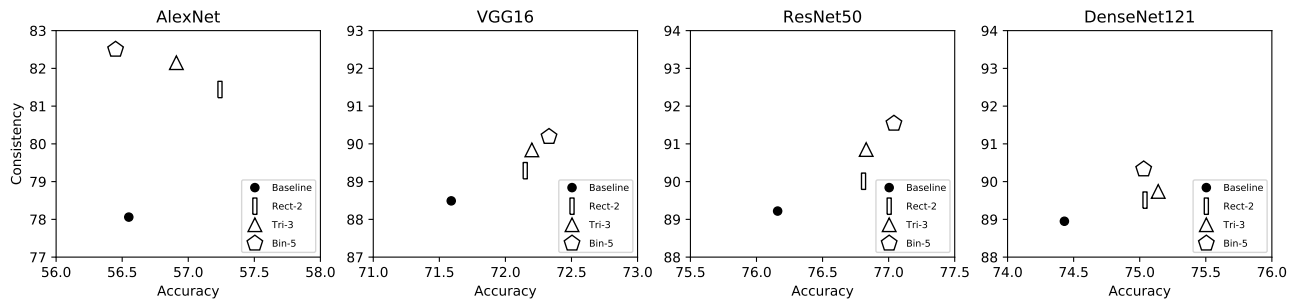

Figure 13. **ImageNet Classification consistency vs. accuracy.** Up (more consistent) and to the right (more accurate) is better. This is the equivalent to Fig. 6 in the main paper, but with each network separately shown in this plot. Note that each axis covers the same dynamic range in each plot (6% for consistency, 2% for accuracy).
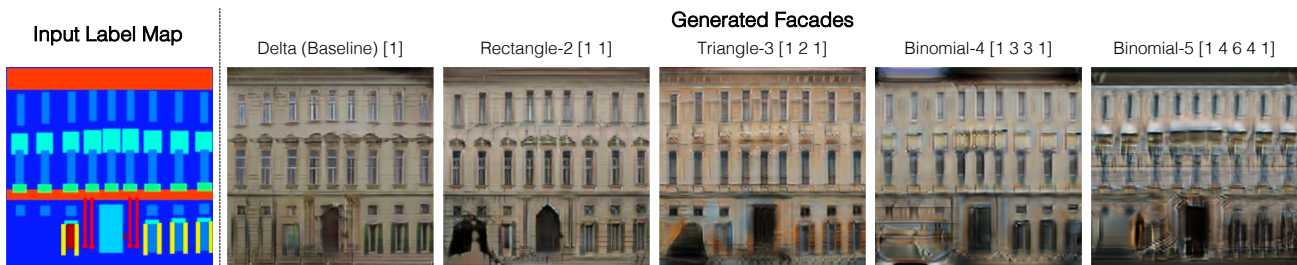

Figure 14. **Example generations.** We show generations with U-Nets trained with 5 different filters. In general, generation quality is well-maintained to *Tri-3* filter, but decreases noticeably with *Bin-4* and *Bin-5* filters due to oversmoothing.